ADVANCED MATERIALS INTERFACES
www.advmatinterfaces.de



# A Fluorescence Probe for Metal Ions Based on Black Phosphorus Quantum Dots

*Zhenyu Xu, Liang Hu, Jun Yuan, Yiyue Zhang, Yujie Guo, Zhengyuan Jin, Fangchao Long, Yaojia Long, Huawei Liang, Shuangchen Ruan, and Yu-Jia Zeng**

**Fluorescence method for detecting metal ions has advantages of fast detection speed, simple operation, and low price over the conventional methods. Black phosphorus quantum dots (BP QDs) have high photoluminescence quantum yield and modifiable surface, which have great potential in the field of fluorescent probes. In this study, high quality BP QDs are prepared by pyrolysis method and are first time used as trace metal ion probes in both organic solutions and aqueous solutions. The detection limits of $Hg^{2+}$ and $Cu^{2+}$ in the aqueous solution are $5.3 \times 10^{-9}$ M and $1.6 \times 10^{-6}$ M, respectively. In addition, the detection limits of $Cu^{2+}$ in the organic solution are $16 \times 10^{-6}$ M. The fluorescence quenching mechanism based on the calculation of the electronic structure and adsorption energy of BP QDs after adsorption of metal ions is further explained. The results provide a new promising fluorescence probe for trace metal ions without the help of organic molecules.**

## 1. Introduction

As the degree of industrialization of human society continues to increase, the threat of the heavy metal ions is growing. The heavy metal ions, such as gold, silver, copper, iron, and lead, as widespread and highly toxic pollutants, enter the atmosphere, water, soil, and human bodies,[1,2] which are difficult to degrade in the environment. Even the concentration is small, the heavy metal ions can accumulate in the algae and the sediment and can be adsorbed by fishes and shellfishes to produce a concentrated food chain, which cause serious health problems such as brain damage, birth defect, renal failure, and immune system damage, DNA damage, and cancer. Therefore, it is of great importance to detect heavy metal ions, in particular to detect trace amounts.[3] Currently, the most reliable detection methods are developed based on the large and sophisticated experimental equipment, such as atomic absorption spectroscopy, X-ray fluorescence, inductively coupled plasma (ICP) mass spectrometry, inductively coupled plasma atomic emission spectroscopy (ICP-AES), and surface plasmon resonance sensing.[4–6] Although these methods have high detection performances, the complicated preprocessing process and the excessive cost limit their range of use and the detection rate. On the other hand, with the advancement of fluorescence technology, fluorescence detection techniques for metal ions by monitoring the fluorescence enhancement, quenching, or shifting of peak positions have attracted great interests. This type of method has advantages of strong visibility, simple operation, wide detection range, and low price.[7] Recently, quantum dot (QD) fluorescent probes are gradually receiving more attentions. Compared with the traditional organic fluorescent materials, QD fluorescent probes have narrower emission spectra, better stability, and photobleaching resistance. For example, carbon QDs,[8,9] CdSe QDs,[10] CdS QDs,[11] perovskites QDs,[12] and a combination of functional molecules and QDs have been studied to detect metal ions such as $Fe^{3+}$, $Pb^{2+}$, $Hg^{2+}$, $Zn^{2+}$, and $Cd^{2+}$.[13–18] However, currently reported fluorescent probes can be used in only one solvent, it is therefore necessary to develop fluorescent probes with strong selectivity, wide detection range, and low detection limit, which can be used in both aqueous and organic solutions.

Black phosphorus (BP) as one of the three major allotropes of phosphorus is a 2D van der Waals material whose atomic layers are stacked by weak van der Waals forces. BP can be stripped into nanosheets down to a single layer or quantum dots with bandgaps varying from 0.3 (bulk BP) to 2.0 eV. Due to this unique property, BP has the size and composition-dependent light absorption, long exciton lifetime, high photoluminescence quantum yield, and ability of surface modification. So far, BP has been used as photothermal agents, photodetectors, photocatalysts, organic photovoltaics, electrocatalysts, and the storage media.[19–24] BP has also been studied in the field of sensors, such as humidity sensors,[25] ratiometric fluorescent probes developed by the surface modification of organic molecules,[26,27] field effect transistor detection of metal ions.[28] In addition, BP has a wide range of applications in the biological field, including the medicine, drug carriers, and cancer treatment.[29–31] In this research, we have successfully prepared black phosphorus quantum dots (BP QDs) with green fluorescence emission, which can directly detect trace $Hg^{2+}$ and $Cu^{2+}$ ions without the help of organic molecules. In particular,

Z. Xu, Dr. L. Hu, J. Yuan, Y. Zhang, Dr. Y. Guo, Dr. Z. Jin, F. Long, Y. Long, Prof. H. Liang, Prof. S. Ruan, Prof. Y.-J. Zeng
Shenzhen Key Laboratory of Laser Engineering
College of Physics and Optoelectronic Engineering
Shenzhen University
Shenzhen 518060, China
E-mail: yjzeng@szu.edu.cn

The ORCID identification number(s) for the author(s) of this article can be found under https://doi.org/10.1002/admi.201902075.

DOI: 10.1002/admi.201902075

 

BP QD probes can be used in both aqueous and organic phases. Compared with other fluorescent QDs, the BP QDs in this study have a number of advantages, including the feasibility of large-scale preparation, low biotoxicity, and good biocompatibility. In addition to the $Hg^{2+}$ in the aqueous solution, BP QDs can also detect $Cu^{2+}$, which are often found in many industrial and daily chemicals, such as, gasoline, cooking oil, skin oil, and lubricating oil.[32] The prepared BP QDs are stored in *N*-methyl-2-pyrrolidone (NMP), which not only provides a long-time protection but also makes it well compatible with organic matters, providing a strategy for detecting metal ions in the organic solution.[33] In addition to the detection of trace metal ions, BP QDs fluorescent probes could be further used in the fields of biological imaging, pH detection, and inorganic detection with proper modifications.[34–36]

## 2. Results and Discussion

### 2.1. Characterization of BP QDs

BP QDs were prepared by pyrolysis method. The experimental procedure is displayed in **Figure 1** and Figure S1 in the Supporting Information. The addition of NaOH and the prolongation of the pyrolysis time can increase the yield of the QDs, which are shown in Figures S2 and S3 in the Supporting Information.[37] The scanning electron microscope (SEM) images of the QDs are shown in Figure S4 in the Supporting Information. However, it is difficult to observe the single BP QD due to the SEM resolution and the agglomeration of the QDs, transmission electron microscope (TEM) was used to further image the QDs. The morphology and size of the BP QDs can be obtained from the TEM image in **Figure 2**a, which confirms the presence of ultrasmall BP QDs. Inset in Figure 2a shows the high-resolution TEM (HRTEM) image of BP QDs in which the lattice fringe is 0.34 nm, corresponding to the (012) plane of BP crystal.[38] According to the statistical TEM analysis of 100 BP QDs, the average lateral size of BP QDs is 2.2 ± 0.4 nm. The X-ray diffraction (XRD) pattern of BP QDs reveals the peaks that are indexed to the (020), (021), (040), (111), (060), and (061) planes in the $2\theta$ range of 10°–70° (powder diffraction file No. 47-1626, Figure S5, Supporting Information). As shown in Figure 2c, Raman peaks of the BP QDs show a redshift as compared to that of bulk BP, which suggest the very small thickness of the BP QDs according to the previous report.[39] The height of the QDs can be derived from the atomic force microscope (AFM) images which is generally less than 2 nm. Note that the long carbon chain and the organic molecules that are liable to adhere to the surface of the QDs might increase the height of the sample. The peak of the UV–vis spectrum shown in Figure 2f indicates that the BP QDs have a thickness of one to two layers. The broad region at 450 nm is consistent with the previous result of BP QDs.[40] Fourier-transform infrared (FT-IR) spectrum and identification of organic groups and chemical bonds are shown in Figure S6 in the Supporting Information. The results are consistent with the previous studies of BP QDs.

### 2.2. Detection of Metal Ions

**Figure 3**a shows photoluminescence (PL) emissions of BP QDs under excitation lights with different wavelengths. During the experiment, the pyrolysis time and the amount of BP were adjusted, which were found not to influence the fluorescence wavelength of the samples. It can be found that the BP QDs

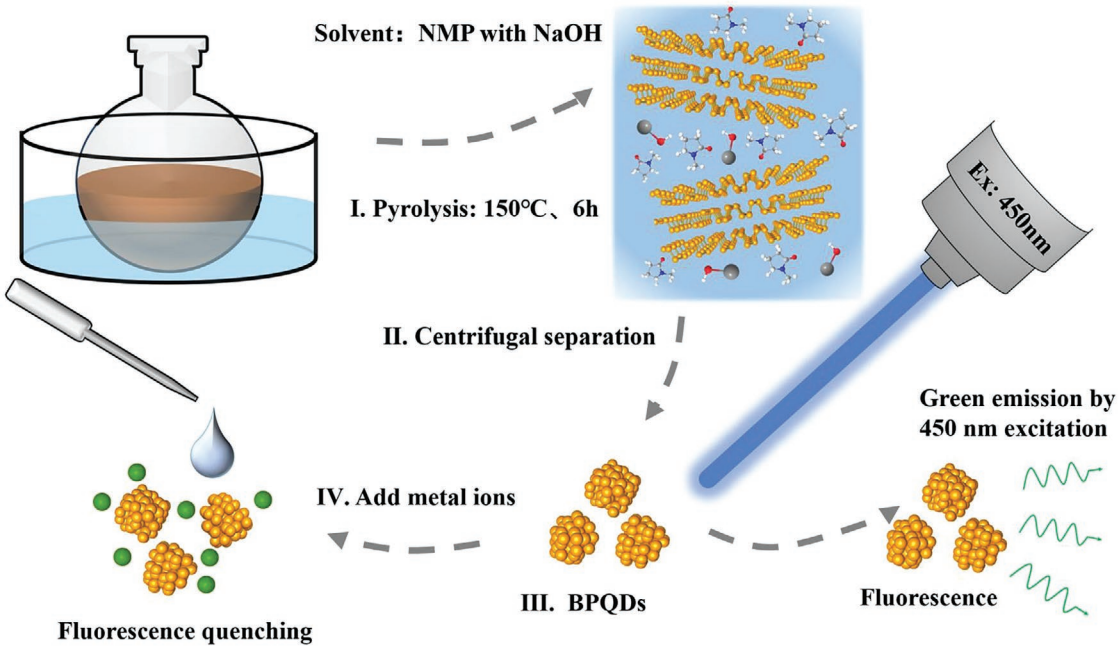


**Figure 1.** Fluorescent BP QDs synthesized through pyrolysis method via a top-down route and the metal ion detection was performed by using a 450 nm laser.

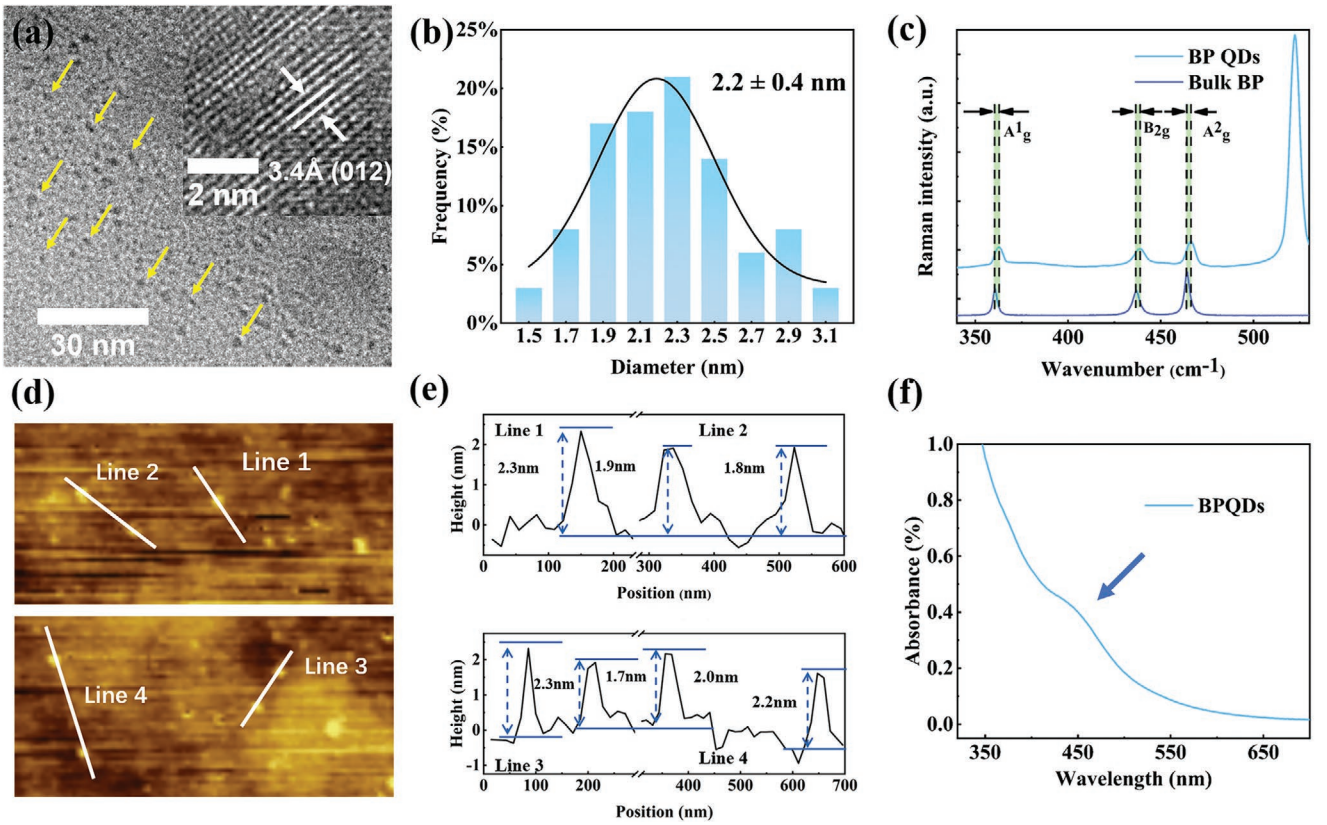


**Figure 2.** a) TEM image of BP QDs. Inset in (a) shows high-resolution TEM (HRTEM) image of BP QDs. b) Statistical analysis of TEM particle size of BP QDs. c) Raman spectroscopy of BP QDs. d) AFM image of BP QDs. e) Statistical of AFM height of BP QD. f) UV–vis absorption spectroscopy of BP QDs.

have the strongest fluorescence intensity under laser excitation at 450 nm. This wavelength dependence also indicates that the PL comes from the quantum size effect of BP QDs.[41,42] In order to avoid the influence of organic solvents on the fluorescence, we performed independent fluorescence tests on the solvent, which is displayed in Figure S7 in the Supporting Information. When the wavelength of the excitation light gradually increases from ultraviolet to visible, the fluorescence of the solvent becomes weak, which indicates that a 450 nm excitation light can avoid the fluorescence range of NMP. Thus, a 450 nm laser is selected for the following detection experiments. The BP QDs prepared by this method have a good stability and their fluorescence can be maintained for more than one month as shown in Figure S8 in the Supporting Information.

Figure 3b is the optical photograph of BP QDs in the NMP solution and the fluorescence image excited by a 450 nm laser. BP QDs prepared in this method can maintain good luminescent properties and stability after mixing with water although they are stored in the organic solvent.[43,44] The quantum efficiency of fluorescence was measured by the FLS 980-STM fluorescence spectrometer. The quantum efficiency is 11.6%, which is higher than the reported $MoS_2$ QDs (4.4%) and carbon QDs (7–11%),[45,46] but still lower than the metal-halide perovskite (14%) and other fluorescent molecules.[47]

Figure 3c,d shows the effect of different metal ions on the fluorescence of BP QDs. In Figure 3c, we select 11 kinds of common metal ions, including $Ag^{2+}$, $Cu^{2+}$, $Hg^{2+}$, $Ca^{2+}$, $Cd^{2+}$, $Ga^{2+}$, $Zn^{2+}$, $In^{2+}$, $Mn^{2+}$, $Al^{3+}$, $Fe^{3+}$, and $Pb^{2+}$. BP QDs without added metal ions are used as comparison and the same amount of BP QDs are used as fluorescent probes to detect metal ions. This experiment is used to verify the selectivity of the fluorescent probes, from which one can find that $Cu^{2+}$ and $Hg^{2+}$ have a larger quenching effect than other metal ions. Figure 3d is a fluorescence experiment conducted on a mixed solution of different metal ions. This experiment is an anti-interference experiment to illustrate that BP QDs fluorescent probe still has good selectivity for $Cu^{2+}$ and $Hg^{2+}$ in the presence of multiple ions.

**Figure 4**a shows PL spectra of BP QDs after mixing with different concentrations of $Hg^{2+}$. It can be seen from the spectra that the fluorescence intensity is gradually weakened with the increase of $Hg^{2+}$ concentration within a certain range. Figure 4c,d is linear fitting curves of different concentration intervals. The coefficients are calculated to be 0.96 and 0.97. The results show a good linear change in the interval of 1–100 and 0.001–1 μg $mL^{-1}$. The detection ranges from 0.001 to 100 μg $mL^{-1}$ ($5.3 \times 10^{-9}$ M to $530 \times 10^{-6}$ M) and the detection limit is down to $5.3 \times 10^{-9}$ M. The detection limit of BP QDs is compared to that of optimized results reported in other QDs as summarized in Table S2 in the Supporting Information. Figure 4f shows the fluorescent photographs of different concentrations of $Hg^{2+}$ ions. It can be seen that as the concentration of $Hg^{2+}$ ions

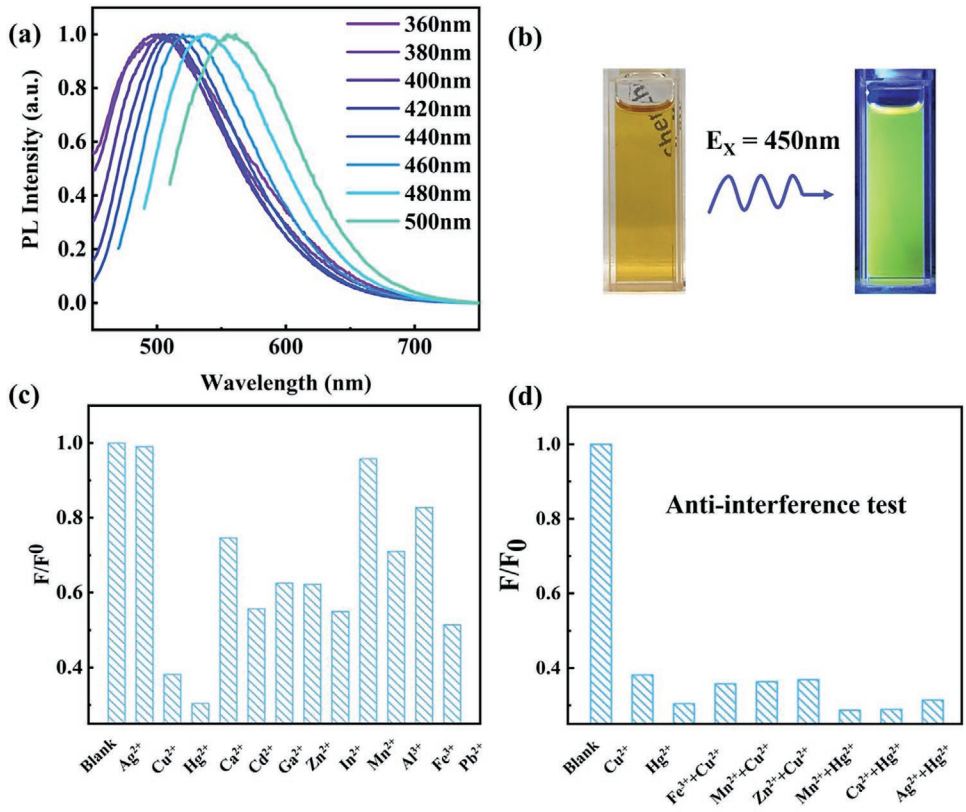


**Figure 3.** a) Normalized excitation-dependent fluorescence spectra of BP QDs. b) Optical photograph of BP QDs in the NMP solution and the fluorescence image excited by a 450 nm laser. c,d) The effect of different metal ions (single and mixture) on the PL intensity of BP QDs. The concentration of metal ions and BP QDs are $80 \times 10^{-6}$ M. The PL peak intensity normalized by the BP QDs without addition of metal ions (the "blank" column).

increases, the fluorescence is continuously weakened under the same intensity of light source.

As mentioned above, fluorescent probes also have a relatively good selective quenching of $Cu^{2+}$. We used probes to detect the concentration of $Cu^{2+}$ in the organic solution. **Figure 5**a shows the fluorescence intensity curves based on the change of $Cu^{2+}$ concentration. Figure 5b shows a linear fit of the change in fluorescence intensity and the determination coefficient is 0.95 in the range of 1–100 μg $L^{-1}$ ($16 \times 10^{-6}$ M–$1.6 \times 10^{-3}$ M), indicating that it has a good linearity, and the detection limit is $16 \times 10^{-6}$ M. Figure 5c is a fluorescent photograph when different concentrations of $Cu^{2+}$ are detected, which also has a good degree of visualization.

Similarly, we also carried out experiments on the fluorescence quenching effect of the $Cu^{2+}$ on BP QDs in the aqueous solution, in which the detection range of copper ions is 0.1–10 μg $mL^{-1}$ ($1.6–160 \times 10^{-6}$ M). The fluorescence quenching still has a good linear coefficient of 0.96. The experimental results are shown in Figure S9 in the Supporting Information. The detection limit of $Cu^{2+}$ in the aqueous solution is improved as compared to that in the organic solution, which may be due to the different diffusion speeds of ions in different solutions. The $Cu^{2+}$ ions in the organic solution have a lower degree of diffusion, resulting in less $Cu^{2+}$ adsorption on the BP QDs in the organic solution.

### 2.3. Mechanism of Fluorescence Quenching

The mechanism of fluorescence quenching was studied by PL lifetime test and X-ray photoelectron spectroscopy (XPS). **Figure 6**a shows the PL lifetime of pure BP QDs and BP QDs mixed with a certain amount of metal ions. By using a biexponential fit, the average lifetime $\tau$ is obtained. The $\tau$ for BP QDs is 10.02 ns. By adding extra metal ions, the $\tau$ measures drastically decrease to 7.84 and 8.96 ns after $Hg^{2+}$ and $Cu^{2+}$ are added, respectively (Table S1, Supporting Information). The decrease of PL lifetime is consistent with the decrease of the fluorescence intensity. The result of PL lifetime indicates that fluorescence quenching is a dynamic quenching mechanism, which suggests that a possible cause of fluorescence quenching is the electron transfer between the metal ion and the BP QDs upon excitation. In general, the fluorescence of BP QDs is thought to come from the quantum size effect, which is also affected by the surface passivation group. Saturated surface functional groups will cause the PL emission wavelength less sensitive to the quantum size effect. In other studies, BP QDs show different emission wavelengths, which result from different functional groups and solvents.[43,48]

To further understand the quenching of fluorescence, XPS measurements were used to study the energy changes between the metal ions and BP QDs. In order to prevent the BP QDs

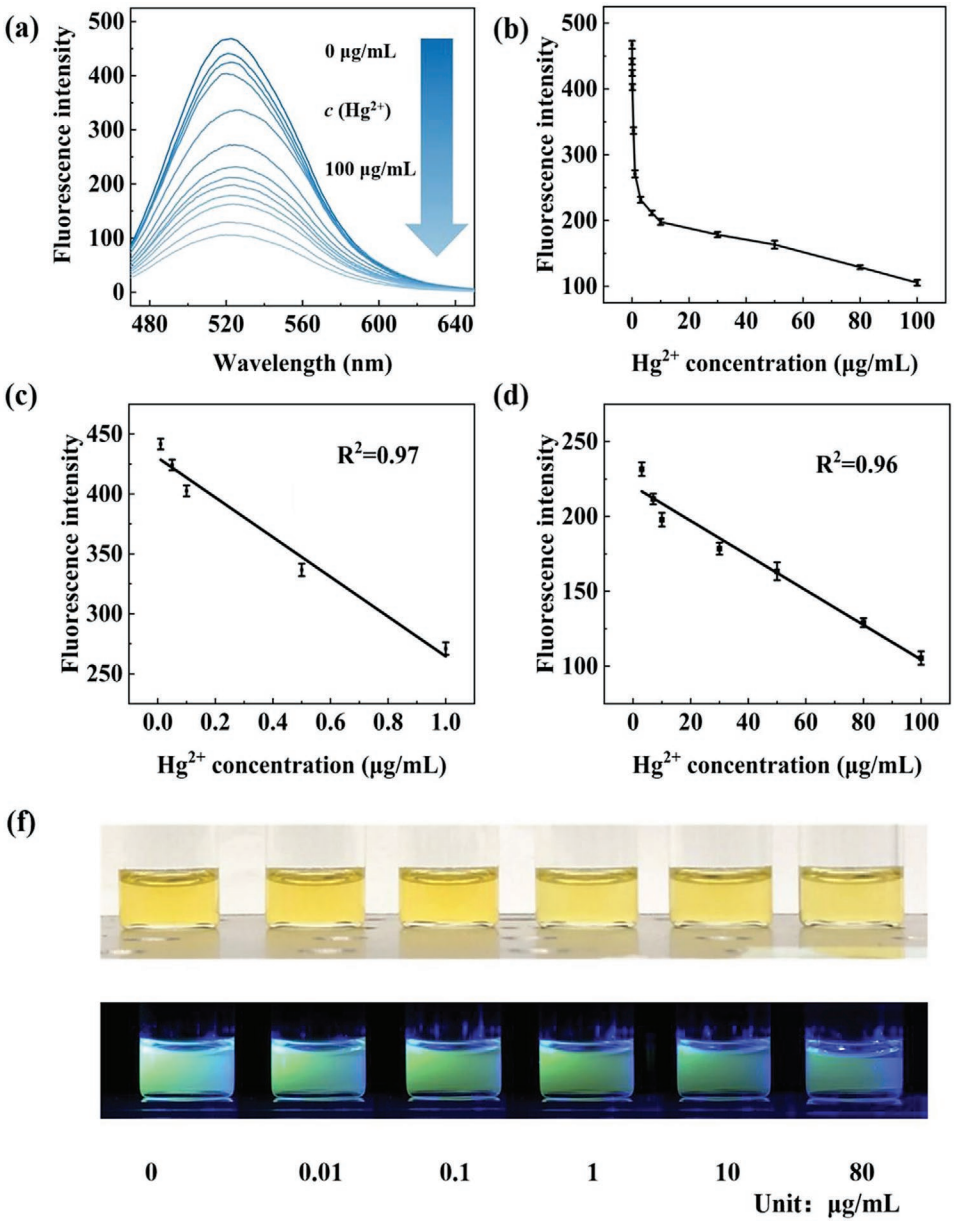


**Figure 4.** a) Fluorescence responses of BP QDs toward different concentrations of $Hg^{2+}$ in the aqueous solution. b–d) Linear plot of the fluorescence intensity at different $Hg^{2+}$ concentrations. f) Optical photos of fluorescence for different concentrations.

from being oxidized, the sample was prepared in a glove box under the nitrogen protection. From P spectra, the peaks at 132.9 eV in the bottom of Figure 6b are attributed to P—O bond, which change to 133.5 and 134.0 eV after $Cu^{2+}$ and $Hg^{2+}$ are added. The shifts are due to the formation of Cu—P and Hg—P bonds.[49] The larger shift of the Hg—P bond might indicate a larger adsorption energy. Correspondingly, the peak at 935.2 and 955.1 eV of Cu2p in Figure 6d and the peak at 102.1 eV of Hg4f in Figure 6e have significant shifts after the adsorption of the BP QDs.[50] The peak positions of Cu2p and Hg4f decrease to 932.6, 952.9, and 99.5 eV, respectively. The results indicate that a charge channel is formed between the metal ions and the BP QDs.

We have further established the adsorption model for $Cu^{2+}$ and $Hg^{2+}$ with BP QDs and calculated the adsorption energy and the charge density.[51] **Figure 7**a,d shows the schematic of adsorption of $Cu^{2+}$ and $Hg^{2+}$ on BP. The detailed structure from different views of the $Cu_{ad}$ and $Hg_{ad}$ are given. In Figures 7b,e, we show the charge density difference of the $Cu_{ad}$–BP and $Hg_{ad}$–BP systems. The blue and yellow regions refer to electron depletion and accumulation, respectively. From the figures, it can be seen that Cu and Hg lose electrons, which means the electrons are transferred to the BP. Enriched electrons are evident between Cu/Hg–P and P–P, which suggests the systems are dominated by covalent bond. Figures 7c,f shows the charge density diagram of the $Cu_{ad}$–BP and $Hg_{ad}$–BP

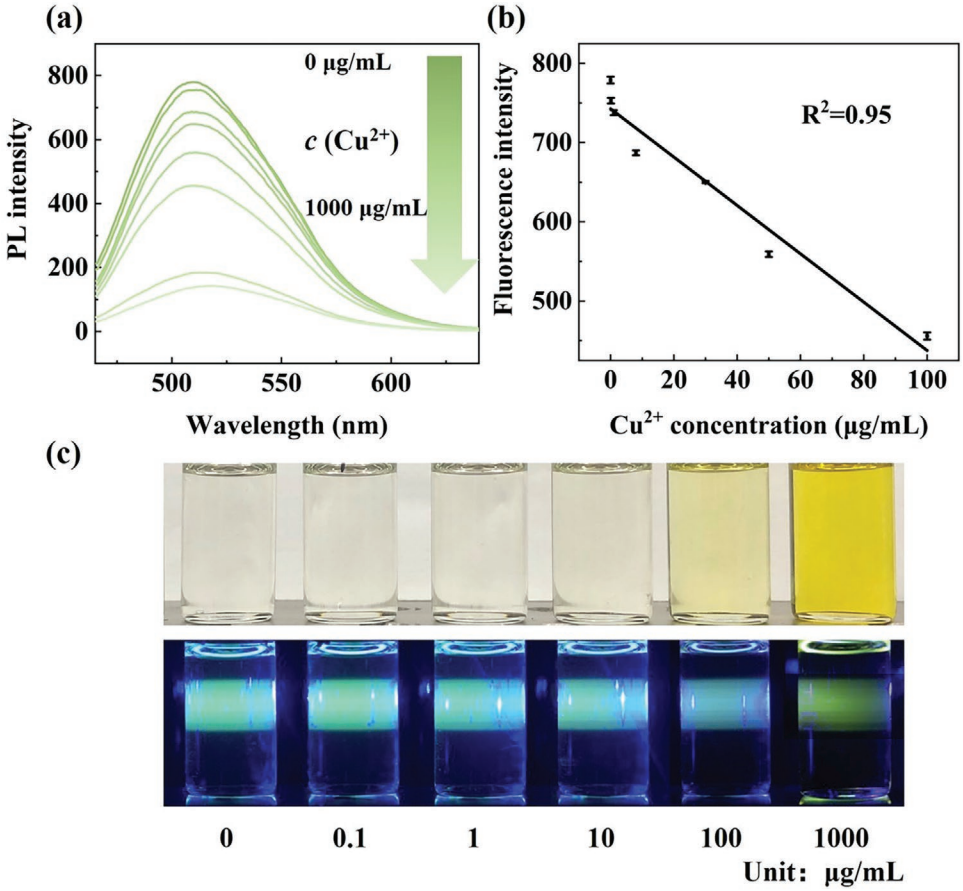


**Figure 5.** a) Fluorescence responses of BP QDs toward different concentrations of $Cu^{2+}$ in the organic solution. b) Linear plot of fluorescence intensity at different $Cu^{2+}$ concentrations. c) Optical photos of fluorescence changes.

systems. From blue to red indicates the increase of the charge density. Since P only has s and p orbital electrons, the charge density of Cu and Hg is higher than that of P.

From the calculation results, the adsorption energy of $Hg^{2+}$ is larger than $Cu^{2+}$, which indicates a stronger bond between Hg and BP. Combined with the results of the electronic structure, it can be seen that the electron transfer between $Hg^{2+}$ and BP is more obvious. These results can explain the larger shift in XPS and better detection performances of $Hg^{2+}$. Most of the previous studies only studied the interaction between BP and atoms. In this study, we have established an adsorption model between BP and metal ions and calculated the electronic structure of BP QDs after adsorption of metal ions. Not only do we further understand and verify the mechanism of the fluorescence quenching of BP QDs caused by metal ions, but also provide a theoretical guidance for the subsequent studies, such as the stability of BP enhanced by metal ions and the influence of metal ions on the electrical properties of BP.

## 3. Conclusion

In summary, we have investigated a fluorescent probe for the detection of trace metal ions in both aqueous and organic phases. The fluorescent BP QDs have been prepared by pyrolysis method, which have been used as fluorescent probes for trace metal ions for the first time. The fluorescence intensity can be maintained for more than one month. The results show that the fluorescent BP QDs can effectively detect $Hg^{2+}$ and $Cu^{2+}$ in the aqueous solution and $Cu^{2+}$ in the organic solution without the assistance of other organic molecules, which have good selectivity in the polluted environment where multiple ions exist simultaneously. Through the PL lifetime and XPS analysis, the fluorescence quenching of BP QDs can be attributed to the charge transfer between the metal ions and BP QDs. Based on the calculation of the electronic structure and adsorption energy, we further explain the difference in fluorescence quenching of BP QDs after adsorption of $Hg^{2+}$ and $Cu^{2+}$. Our results shed light on BP QDs as promising fluorescent probe for trace metal ions.

## 4. Experimental Section

*Materials*: NMP (99.9%, anhydrous), sodium hydroxide (NaOH), $CuCl_2{\cdot}2H_2O$ and the standard aqueous solutions of $Hg(NO_3)_2$, $Fe(NO_3)_2$, $Cd(NO_3)_2$, $Cu(NO_3)_2$, $Mn(NO_3)_2$, $Ca(NO_3)_2$, $Co(NO_3)_2$, $In(NO_3)_3$, $Al(NO_3)_3$, $Ga(NO_3)_3$, $Ag(NO_3)_2$, and $Zn(NO_3)_2$ were purchased from Aladdin company (Shanghai, China). BP crystals were obtained from Xianfeng Nano Materials Tech Co. Ltd. (Nanjing, China). All the materials were used as received without any further purification.

*Preparation of BP QDs*: BP crystals were first grinded into the powder and added into a bottle with NMP solution. 5 mg bulk BP was dispersed

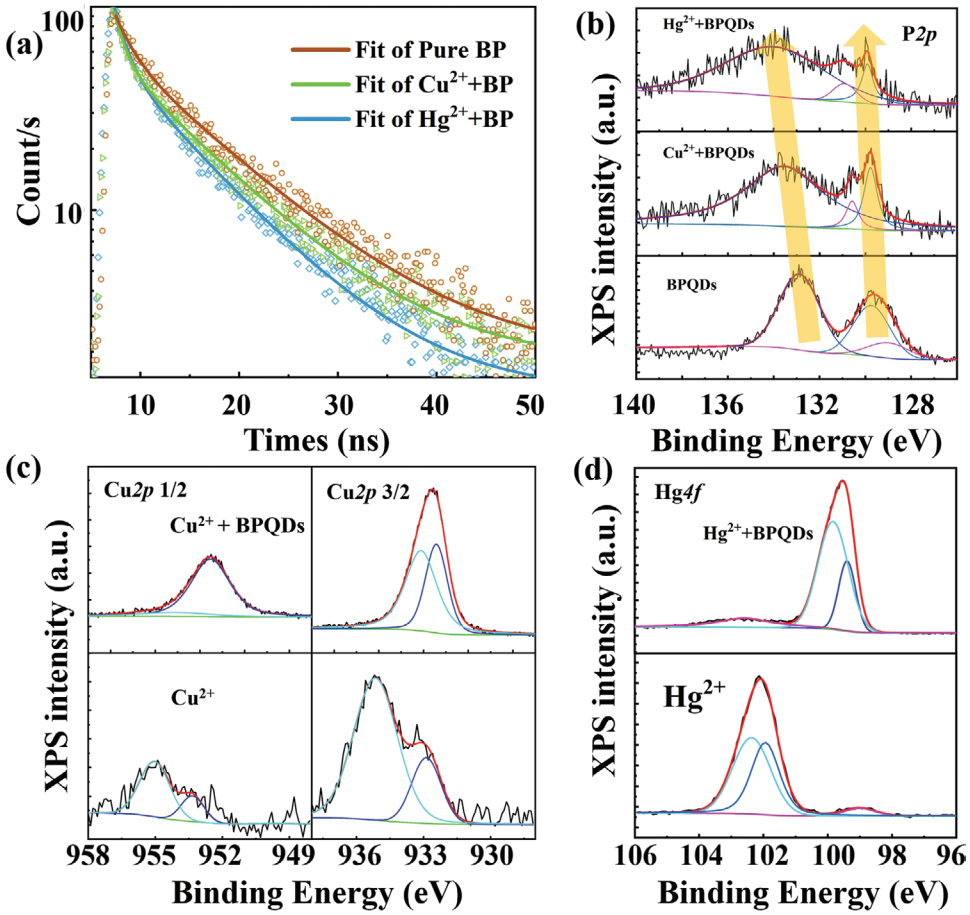


**Figure 6.** a) Fluorescence decay of BP QDs and the mixture of metal ions and BP QDs. b–d) XPS of metal ions and BP QDs after adding of metal ions.

in 50 mL NMP solvent with 20 mg NaOH and then held under vigorous stirring for 6 h at 150 °C under the protection of $N_2$. During the process, the solution was gradually turned to light yellow. Afterward, the resulting suspensions were separated and purified by stepwise centrifugation 6000, 9000, and 16 000 rpm.

*Detection of Metal Ions*: By mixing a certain amount of BP QDs (50 µL, 0.25 mg $mL^{-1}$) with heavy metal ions (30 µL) of different concentrations, the mixture was shaken and equilibrated for 3 min. The fluorescence intensity was measured using a 450 nm laser. The aqueous solution of metal ions was prepared by diluting a standard solution of metal ions with deionized water. The $Cu^{2+}$ organic solution was prepared by dispersing copper chloride in the NMP solution

*Characterization*: Fluorescence measurements were carried out by using a SHIMADZU RF-5301PC spectrofluorometer. The thickness of the BP QDs was calculated by using advanced integrated scanning tools SmartSPM 1000 Scanning Probe Microscope combined with atomic force module. The crystalline quality and structural properties were characterized by TEM images and were recorded using an Fédération Equestre Internationale Tecnai G2 F30 and high-resolution transmission electron microscope operating at 200 kV. The surface morphology of BP QDs was measured by SEM (Carl Zeiss MERLIN compact). FT-IR spectroscopy measurements were carried out on a Nicolet iS50 in the 400–4000 $cm^{-1}$ wavenumber range. UV–vis spectra were measured using a Shimadzu UV-2600 UV–vis spectrophotometer. Time-resolved PL measurements and the quantum efficiency of fluorescence were conducted in Edinburgh Instruments FLS 980-STM fluorescence spectrophotometer using a picosecond pulsed diode laser ($\lambda$ = 450 nm) as the excitation source. XPS studies were carried out on an ESCALAB 250XI (Thermo Scientific) using Al $K_\alpha$ monochromatic source (1486.6 eV). XRD measurements were carried out with a Rigaku SmartLab X-ray diffractometer (Cu KR radiation $\lambda = 1.54056$ Å) operating at 45 kV and 200 mA. The concentrations of BP QDs dispersions were determined by ICP-AES (PerkinElmer OPTIMA2100DV). The Raman scattering spectra were collected by a Raman spectrometer (HORIBA LabRAM HR Evolution). The excitation wavelength was 514.5 nm.

*Computational Methods*: The Vienna Ab initio simulation package (VASP) software was used in the density functional theory calculation to simulate the adsorption of $Cu^{2+}$ and $Hg^{2+}$ on the surface of black phosphorus according to the charged system. The model of monolayer phosphorene was constructed by using 60 atoms.[52,53] The model and the results of the electronic structure are reflected in Figure 7. All the geometry optimization in this work were performed with the VASP code,[54] using the generalized gradient approximation in the form of the Perdew–Burke–Ernzerhof[55] exchange-correlation functional. The projected augmented wave method[56] was used to describe the interaction between the valence electrons and the core. The Monkhorst–Pack[57] scheme was applied in order to sample the Brillouin zone, and the plane wave kinetic energy cutoff was set at 500 eV, and a corresponding $2 \times 2 \times 1$ $k$-points mesh was used during optimization. The adsorption energy $\Delta E_{ad}$ was calculated using

$$\Delta E_{ad} = E_{(BP+X)} - E_{BP} - E_X \quad (1)$$

where $E_{(BP+X)}$ was the total energy of BP with 1 Cu or Hg atom adsorbed on the facet, $E_{BP}$ was the total energy of BP, $E_X$ was the total energy of $Cu^{2+}$ or $Hg^{2+}$. The adsorption energies of $Cu^{2+}$ at BP facet were −58.39021954923084 kcal. The adsorption energies of $Hg^{2+}$ at BP facet were −160.3795332371489 kcal. The lower adsorption energy suggested the stronger adsorb.

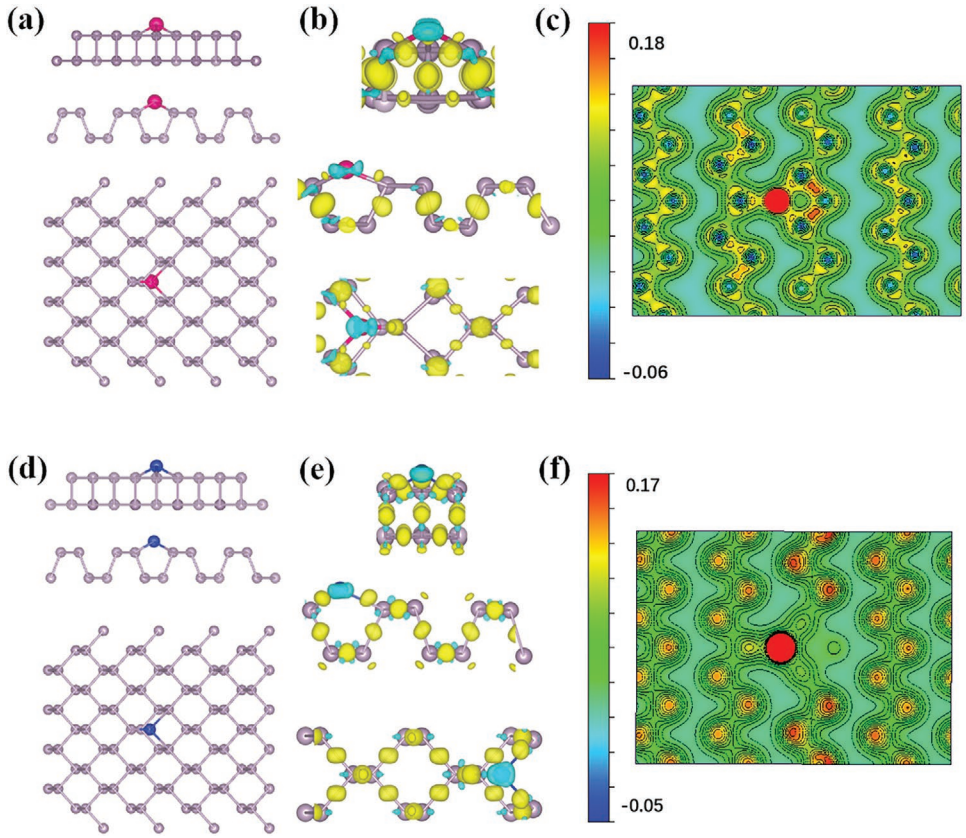


**Figure 7.** a,d) Schematic of adsorption of $Cu^{2+}$ and $Hg^{2+}$ on BP QDs. Three different views of the structure. The silver sphere: P atom, the blue sphere: Cu atom, and the pink sphere: Hg atom. b,d) Charge density difference of the $Cu_{ad}$ and $Hg_{ad}$. The blue and yellow regions refer to electron depletion and accumulation, respectively. c,e) Charge density diagram of the $Cu_{ad}$ and $Hg_{ad}$ (isosurface 0.1 e $bohr^{-3}$).

## Supporting Information

Supporting Information is available from the Wiley Online Library or from the author.

## Acknowledgements

This work was supported by the National Natural Science Foundation of China under Grant Nos. 11874270 and 61804098, the Shenzhen Science and Technology Project under Grant Nos. JCYJ20170412105400428 and JCYJ20180507182246321, and the Shenzhen Peacock Technological Innovation Project under Grant No. KQJSCX20170727101208249.

## Conflict of Interest

The authors declare no conflict of interest.

## Keywords

black phosphorus, electron transfer, fluorescence, metal ions

Received: December 10, 2019
Revised: January 18, 2020
Published online: February 11, 2020

[1] J. E. Holland, A. E. Bennett, A. C. Newton, P. J. White, B. M. McKenzie, T. S. George, R. J. Pakeman, J. S. Bailey, D. A. Fornara, R. C. Hayes, *Sci. Total Environ.* **2018**, *610–611*, 316.
[2] P. T. Lieu, M. Heiskala, P. A. Peterson, Y. Yang, *Mol. Aspects Med.* **2001**, *22*, 1.
[3] M. Bundschuh, J. Filser, S. Luderwald, M. S. McKee, G. Metreveli, G. E. Schaumann, R. Schulz, S. Wagner, *Environ. Sci. Eur.* **2018**, *30*, 6.
[4] D. V. Biller, K. W. Bruland, *Mar. Chem.* **2012**, *130–131*, 12.
[5] M. Ghaedi, M. Reza Fathi, A. Shokrollahi, F. Shajarat, *Anal. Lett.* **2006**, *39*, 1171.
[6] N. F. Lokman, A. A. A. Bakar, F. Suja, H. Abdullah, W. B. W. Ab Rahman, N.-M. Huang, M. H. Yaacob, *Sens. Actuators, B* **2014**, *195*, 459.
[7] D. Wu, A. C. Sedgwick, T. Gunnlaugsson, E. U. Akkaya, J. Yoon, T. D. James, *Chem. Soc. Rev.* **2017**, *46*, 7105.
[8] N. Gogoi, M. Barooah, G. Majumdar, D. Chowdhury, *ACS Appl. Mater. Interfaces* **2015**, *7*, 3058.
[9] N. Murugan, M. Prakash, M. Jayakumar, A. Sundaramurthy, A. K. Sundramoorthy, *Appl. Surf. Sci.* **2019**, *476*, 468.
[10] T. Sung, Y. Lo, *Sens. Actuators, B* **2012**, *165*, 119.
[11] C. Boonmee, T. Noipa, T. Tuntulani, W. Ngeontae, *Spectrochim. Acta, Part A* **2016**, *169*, 161.
[12] X. Sheng, Y. Liu, Y. Wang, Y. Li, X. Wang, X. Wang, Z. Dai, J. Bao, X. Xu, *Adv. Mater.* **2017**, *29*, 1700150.
[13] Z. Zhou, R. Yan, J. Zhao, L. Yang, J. Chen, Y. Hu, F. Jiang, Y. Liu, *Sens. Actuators, B* **2018**, *254*, 8.
[14] W. Zhang, B. Shan, D. Liang, Y. Shi, D. Han, C. Huang, *Anal. Methods* **2016**, *8*, 7762.

[15] Y. Wang, S. Lao, W. Ding, Z. Zhang, S. Liu, *Sens. Actuators, B* **2019**, *284*, 186.
[16] X. Niu, Y. Zhong, R. Chen, F. Wang, Y. Liu, D. Luo, *Sens. Actuators, B* **2018**, *255*, 1577.
[17] M. Zhou, J. Guo, C. Yang, *Sens. Actuators, B* **2018**, *264*, 52.
[18] Y. Ding, H. Yin, M. M. Musameh, X. Hao, I. L. Kyratzis, S. Shirley, K. Sun, F. Liu, *New J. Chem.* **2018**, *42*, 4871.
[19] Z. Sun, H. Xie, S. Tang, X. F. Yu, Z. Guo, J. Shao, H. Zhang, H. Huang, H. Wang, P. K. Chu, *Angew. Chem., Int. Ed.* **2015**, *54*, 11526.
[20] N. Youngblood, C. Chen, S. J. Koester, M. Li, *Nat. Photonics* **2015**, *9*, 247.
[21] J. Wu, S. Huang, Z. Jin, J. Chen, L. Hu, Y. Long, J. Lu, S. Ruan, Y. Zeng, *J. Mater. Sci.* **2018**, *53*, 16557.
[22] S. Liu, S. Lin, P. You, C. Surya, S. P. Lau, F. Yan, *Angew. Chem., Int. Ed.* **2017**, *56*, 13717.
[23] Q. Jiang, L. Xu, N. Chen, H. Zhang, L. Dai, S. Wang, *Angew. Chem., Int. Ed.* **2016**, *55*, 13849.
[24] L. Hu, J. Yuan, Y. Ren, Y. Wang, J. Q. Yang, Y. Zhou, Y. J. Zeng, S. T. Han, S. Ruan, *Adv. Mater.* **2018**, *30*, 1801232.
[25] C. Zhu, F. Xu, L. Zhang, M. Li, J. Chen, S. Xu, G. Huang, W. Chen, L. Sun, *Chem. - Eur. J.* **2016**, *22*, 7357.
[26] W. Gu, X. Pei, Y. Cheng, C. Zhang, J. Zhang, Y. Yan, C. Ding, Y. Xian, *ACS Sens.* **2017**, *2*, 576.
[27] W. Gu, Y. Yan, X. Pei, C. Zhang, C. Ding, Y. Xian, *Sens. Actuators, B* **2017**, *250*, 601.
[28] P. Li, D. Zhang, C. Jiang, X. Zong, Y. Cao, *Biosens. Bioelectron.* **2017**, *98*, 68.
[29] C. A. Flemming, J. T. Trevors, *Water, Air, Soil Pollut.* **1989**, *44*, 143.
[30] L. Hu, M. N. Amini, Y. Wu, Z. Jin, J. Yuan, R. Lin, J. Wu, Y. Dai, H. He, Y. Lu, J. Lu, Z. Ye, S. Han, J. Ye, B. Partoens, Y. Zeng, S. Ruan, *Adv. Opt. Mater.* **2018**, *6*, 1800440.
[31] C. Xing, S. Chen, M. Qiu, X. Liang, Q. Liu, Q. Zou, Z. Li, Z. Xie, D. Wang, B. Dong, L. Liu, D. Fan, H. Zhang, *Adv. Healthcare Mater.* **2018**, *7*, 1701510.
[32] M. Qiu, D. Wang, W. Liang, L. Liu, Y. Zhang, X. Chen, D. K. Sang, C. Xing, Z. Li, B. Dong, F. Xing, D. Fan, S. Bao, H. Zhang, Y. Cao, *Proc. Natl. Acad. Sci. U. S. A.* **2018**, *115*, 501.
[33] M. Qiu, W. X. Ren, T. Jeong, M. Won, G. Y. Park, D. K. Sang, L. P. Liu, H. Zhang, J. S. Kim, *Chem. Soc. Rev.* **2018**, *47*, 5588.
[34] S. Liao, X. Huang, H. Yang, X. Chen, *Anal. Bioanal. Chem.* **2018**, *410*, 7701.
[35] L. Wang, B. Wu, W. Li, S. Wang, Z. Li, M. Li, D. Pan, M. Wu, *Adv. Biosyst.* **2018**, *2*, 1700191.
[36] Y. Tian, L Hao, C. Wang, X. Yang, S. Liu, *Nanomaterials* **2019**, *9*, 111.
[37] Z. Guo, H. Zhang, S. Lu, Z. Wang, S. Tang, J. Shao, Z. Sun, H. Xie, H. Wang, X. Yu, P. K. Chu, *Adv. Funct. Mater.* **2015**, *25*, 6996.
[38] X. Zhang, H. Xie, Z. Liu, C. Tan, Z. Luo, H. Li, J. Lin, L. Sun, W. Chen, Z. Xu, L. Xie, W. Huang, H. Zhang, *Angew. Chem., Int. Ed.* **2015**, *54*, 3653.
[39] A. Favron, F. A. Goudreault, V. Gosselin, J. Groulx, M. Cote, R. Leonelli, J. F. Germain, A. L. Phaneuf-L'Heureux, S. Francoeur, R. Martel, *Nano Lett.* **2018**, *18*, 1018.
[40] Y. J. Yuan, S. Yang, P. Wang, Y. Yang, Z. Li, D. Chen, Z. T. Yu, Z. G. Zou, *Chem. Commun.* **2018**, *54*, 960.
[41] A. Castellanos-Gomez, L. Vicarelli, E. Prada, J. O. Island, K. L. Narasimha-Acharya, S. I. Blanter, D. J. Groenendijk, M. Buscema, G. A. Steele, J. V. Alvarez, H. W. Zandbergen, J. J. Palacios, H. S. J. van der Zant, *2D Mater.* **2014**, *1*, 025001.
[42] H. Lee, S. Park, S. Lee, S. Choi, S. Seo, H. Kim, J. Won, K. Choi, K. S. Kang, H. Park, H. Kim, H. R. An, K. Jeong, Y. Lee, J. Lee, *Small* **2016**, *12*, 214.
[43] L. Long, X. Niu, K. Yan, G. Zhou, J. Wang, X. Wu, P. K. Chu, *Small* **2018**, *14*, 1803132.
[44] D. Hanlon, C. Backes, E. Doherty, C. S. Cucinotta, N. C. Berner, C. Boland, K. Lee, A. Harvey, P. Lynch, Z. Gholamvand, S. Zhang, K. Wang, G. Moynihan, A. Pokle, Q. M. Ramasse, N. McEvoy, W. J. Blau, J. Wang, G. Abellan, F. Hauke, A. Hirsch, S. Sanvito, D. D. O'Regan, G. S. Duesberg, V. Nicolosi, J. N. Coleman, *Nat. Commun.* **2015**, *6*, 8563.
[45] H. Lin, C. Wang, J. Wu, Z. Xu, Y. Huang, C. Zhang, *New J. Chem.* **2015**, *39*, 8492.
[46] L. Tang, R. Ji, X. Cao, J. Lin, H. Jiang, X. Li, K. S. Teng, C. M. Luk, S. Zeng, J. Hao, S. P. Lau, *ACS Nano* **2012**, *6*, 5102.
[47] Y. Zhang, C.-K. Lim, Z. Dai, G. Yu, J. W. Haus, H. Zhang, P. N. Prasad, *Phys. Rep.* **2019**, *795*, 1.
[48] S. Ge, L. Zhang, P. Wang, Y. Fang, *Sci. Rep.* **2016**, *6*, 27307.
[49] Z. Guo, S. Chen, Z. Wang, Z. Yang, F. Liu, Y. Xu, J. Wang, Y. Yi, H. Zhang, L. Liao, P. K. Chu, X. F. Yu, *Adv. Mater.* **2017**, *29*, 1703811.
[50] L. Hu, L. Zhu, H. He, Y. Guo, G. Pan, J. Jiang, Y. Jin, L. Sun, Z. Ye, *Nanoscale* **2013**, *5*, 9577.
[51] S. P. Koenig, R. A. Doganov, L. Seixas, A. Carvalho, J. Y. Tan, K. Watanabe, T. Taniguchi, N. Yakovlev, A. H. Castro Neto, B. Ozyilmaz, *Nano Lett.* **2016**, *16*, 2145.
[52] R. Hultgren, N. Gingrich, B. Warren, *J. Chem. Phys.* **1935**, *3*, 351.
[53] A. Prakash, Y. Cai, G. Zhang, Y. W. Zhang, K. W. Ang, *Small* **2017**, *13*, 1602909.
[54] G. Kresse, J. Furthmuller, *Phys. Rev. B* **1996**, *54*, 11169.
[55] J. P. Perdew, K. Burke, M. Ernzerhof, *Phys. Rev. Lett.* **1996**, *77*, 3865.
[56] P. E. Blochl, *Phys. Rev. B: Condens. Matter Mater. Phys.* **1994**, *50*, 17953.
[57] H. J. Monkhorst, J. D. Pack, *Phys. Rev. B* **1976**, *13*, 5188.